G 1/3

# On the Measurement of CTOD in Ductile Steels Using Glass Fibres

C. Zimmermann, T. Demler

*Universität Stuttgart, Staatliche Materialprüfungsanstalt (MPA), Pfaffenwaldring 32, D-7000 Stuttgart 80, Germany*

## Abstract

A glass-fibre sensor was used for the acquisition of CTOD in standard CT-specimens of ductile steels. The fibres were positioned up to a distance of 1 mm behind the tip of the fatigue crack in the mid-thickness section. CTOD could be measured with a resolution of better than 1 µm. Experiments were performed at temperatures between RT and 80 °C with the intention of verifying the British Standard BS 5762 when measuring inside the CT-specimen. Results as gained in course of this investigation confirm the BS 5762 extrapolation technique.

## 1. Introduction

For ductile materials the COD-concept has become commonly accepted as a failure criterion, since it is applicable for any temperature or toughness level. Analogously to the near-tip parameter $K_{Ic}$ of Linear Elastic Fracture Mechanics, this concept uses the critical crack tip opening displacement CTOD to characterize the resistance of ductile materials to crack initiation.

To this end, numerical or experimental data on CTOD as gained from standardized specimens are needed. However, due to the very shape of the crack tip numerous definitions exist of what CTOD means and where it is to be measured /1,2,3/. Of these, the procedure as laid down in the BS 5762 proved successful and will thus be used throughout this paper, too.

Since an actual continuous measurement of CTOD in the specimen center (i.e. where crack initiation starts first) did not seem possible with the known experimental tools, an extrapolation formalism was given by BS 5762 to calculate CTOD from easily performable COD-measurements, assuming for the calculation of plastic deformation even crack fronts up to the crack tip.

$$CTOD = \frac{K^2\,(1-\mu^2)}{2E \cdot R_e} + \frac{0{,}4\,(W-a)}{0{,}4 \cdot W + 0{,}6 \cdot a} \cdot V_{pl} \qquad (1)$$

This, however, cannot be true exactly, due to the tri-axial stress/strain state at the crack tip.

Now to describe the characteristics of the specimen, the experimentally determined J-values are plotted versus the measured load-line COD, a graph which by virtue is of parabolic shape, inducing growing errors of J as COD rises. As a consequence, J-controlled experiments are rather difficult. On the other hand, the simple BCS-Dugdale model, as well as e.g. recent 3D-FEM analyses by Wellman et al. /4/ suggest a linear relationship between J and CTOD, which would be advantageous in many ways. Moreover, in case of dynamic testing, the inevitable inertia effects ask for CTOD-measurements in the specimen center in order to get a correct material characterization. Therefore, a new CTOD-meter using a fibre guided laser beam has been developed at the MPA Stuttgart, whose perfomance will be described in the following.

## 2. Experimental setup

In principle, the sensor consists of two glass-fibres inserted end to end into the specimen some 1 to 3 mm away from the fatigue crack tip through a drilling hole of 0,9 mm diameter, Fig. 1. For the experiments described hereafter, CT-25 specimens were used with the sensor being situated in the specimen mid thickness location. Several prototypes were tested of which the final configuration was then taken for testing. The sensor meets the following specifications:

| | |
|---|---|
| Temperature range:<br>(Fibre dependent) | $-20\ ^{o}C$ to $+350\ ^{o}C$ (8 h) |
| Dynamic range: | 0 to 10 MHz |
| Local resolution:<br>(Fibre dependent) | lateral < 5.0 μm<br>axial < 1 μm |
| Measuring range:<br>(Fibre dependent) | 0 ... 2000 μm (at 10 MHz) |
| Dimensions,<br>sensor head: | diameter 0,9 mm, length 200 mm |

With the fibre axes oriented vertically to the crack plane the lateral measuring position might be anywhere inside the specimen. Multiple simultaneous measurements along the crack front are possible with an adequate number of sensors. After insertion into the specimen each sensor is calibrated parallel to its axis using micropositioning gauges clamped to the upper or lower side of the specimen. After calibration the two fibre ends are fixed to the flanks of the fatigue crack in the specimen interior. For the measurement of the rising distance between the crack flanks (and consequently the fibre ends) a laser beam which is coupled into the fibres is used. For a further understanding of the measuring principles some remarks on the mechanisms of light travel within a fibre seem useful.

Glass fibres, originally developed for broadband data-transmission lines in the far GHz-region are now available in various customer-oriented specifications, Fig. 2. Basically, a fibre in its most simple configuration consists of a glass core of 5 µm Ø to 150 µm Ø and a glass clad of about 100 µm to 1 mm outer Ø. Core and clad have slightly different refractive indices thus forcing a light beam once coupled into the fibre to follow the fibre due to Snellius law. Due to the same law, however, only light hitting the fibre end within a certain spatial angle $\theta_A$ will be accepted (and emitted again by the other fibre end). The spatial intensity distribution of the emitted light will then be

$$\varphi = \varphi_o \cdot \frac{\cos^2\theta}{r^2} \quad ; \quad r > \text{core-diameter} \qquad (2)$$

with $\varphi_o$ being the original intensity of the fibre-transmitted light, $\theta \leq \theta_A$ being the spatial angle and r being the distance between detector and fibre end. If the detector is a second fibre, whose end is at a distance r from the emitting fibre ( as it is true for the CTOD-meter) the detected intensity will be

$$\emptyset = \int_{-\Omega}^{+\Omega} \varphi(\theta, r) \quad . \quad Z(\theta,\Omega,r)\, d\Omega \qquad (3)$$

with $\sin\theta_A$, $\sin\Omega_A$ being the respective numerical apertures of the two fibres, $Z(\theta,\Omega,r)$ a second order disturbance function which accounts for possible fibre axes misalignments and stray light effects. Equation (3) is used by the CTOD-sensor for the measurement of the crack flanks distance. Because of $Z(\theta,\Omega,r)$ and the inevitable manufacturing tolerances of the specimen the system has to be calibrated after insertion into the specimen for the demanded accuracy of < 1 µm. Fig. 3 shows the calibration curves of various real specimens. To demonstrate a possible angle influence the sensor was mounted onto a precision angular meter, the results are illustrated in Fig. 4. As can be taken from both figures the $1/r^n$-singularity results in a high spatial resolution for small values of r, whereas the angular dependency is negligible in the range of the expected angular specimen movement (+5 ° ... -5 °). The true material parameter CTOD was found by a linear extrapolation from the COD clip gauge signal and the glass fibre signal to the crack tip position. The extrapolated value is denoted $CTOD_{ex}$ and will be compared with the result of eq. (1), denoted $CTOD_{BS}$.

## 3. Test Results

Ten specimens of three different reactor pressure vessel steels, a 20 MnMoNi 55, a 22 NiMoCr 37 (both forged) and a 20 MnMoNi 55 (weld metal) were available for the tests. The respective testing temperatures were 60 $^{o}C$, 80 $^{o}C$ and RT in the upper transition or upper shelf region of the Charpy impact test, cf. Fig. 5. Some representative results are presented in Figs. 6 to 10. In Fig. 6 the usual F-COD relation as obtained by the tests is redrawn. In Fig. 7 the respective $CTOD_{ex}$-COD curves are given. A linear relationship between $CTOD_{ex}$ and COD exists only for COD > 0,6 mm. For comparison purposes an additional curve is inserted into the graph, which has been calculated by Wellman et al. /4/ for a three point-bending specimen of A 508-steel (22 NiMoCr 37) using 3D elasto-plastic FEM-analysis. This curve shows the same tendency. The experimentally determined results for A 508 show a still better coincidence with our results. The agreement is further supported by the graphs in Fig. 8, where CTOD according to BS 5762 is compared with the extrapolated $CTOD_{ex}$-signal. Ideally, a straight 45 $^{o}$-line should be found. Actually, this is true for CTOD-values greater than 80 µm. The most interesting findings are illustrated in Fig. 9 and Fig. 10. While Fig. 9 represents the well-known parabolic relation of J and COD, the same J-values plotted versus the $CTOD_{ex}$-values result in straight lines of various slopes in Fig. 10. For comparison purposes the values given by Wellman et al. are plotted in the same graph. A small disturbancy exists for very small CTOD-values as could be expected, for the however greatest part the linear relationship already postulated by the simple BCS-Dugdale model holds:

$$J = m \cdot R_e \cdot CTOD \qquad 1<m<2 \qquad (4)$$

## 4. Conclusions

The experiments performed on standard CT 25 specimens with a newly developed glass fibre CTOD-meter allowed the continuous acquisition of CTOD within the specimen interior. The linear relationship of J and CTOD as postulated by the BCS-Dugdale-model could be confirmed. Recently proposed corrections /5/ of the BS 5762-extrapolation proved not to be necessary.

## References

/1/ Harrison, J. D. "The State of the Art in Crack Tip Opening Displacement (CTOD) Testing and Analysis" Metal Construct. 12, Sept. - Nov. 1980

/2/ Burdekin, F. M., Stone, D. E. W. "The Crack Opening Displacement Approach to Fracture Mechanics in Yielding Materials", J.Strain Anal. Vol. 1, No. 2, 1966, pp 145-153

/3/ Rice, J. R. "A Path Independent Integral and the Approximate Analysis of Strain Concentration by Notches and Cracks", J. Appl. Mech., Trans. ASME, 35, June 1968

/4/ Wellman, G. W., Rolfe, S. T., Dodds, R. H. "Three-Dimensional Elastic-Plastic Finite Element Analysis of Three-Point Bend Specimens", WRC-bulletin 299, November 1984, pp. 15-25

/5/ Matsoukas, G., Cotterell, B., Mai, Y. W. "On the plastic rotation constant used in Standard COD Tests", Int. J. Fract. 26 (1984), R 49 - R 53


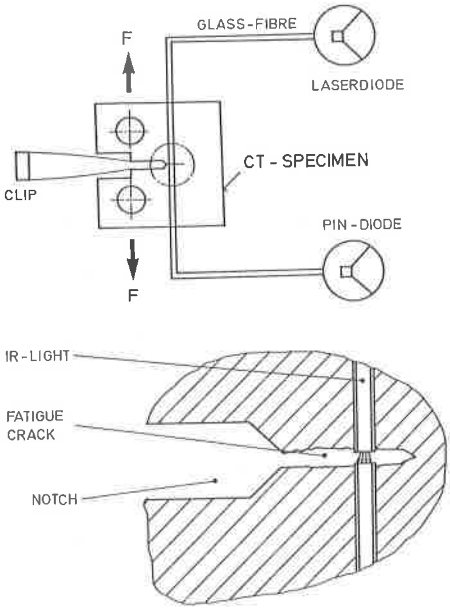


Fig. 1: CTOD-meter, principle

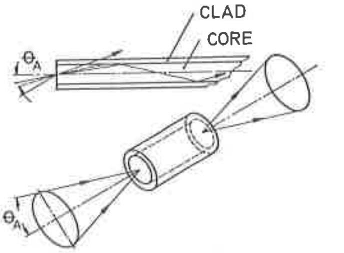


Fig. 2: Light travel in a glass-fibre

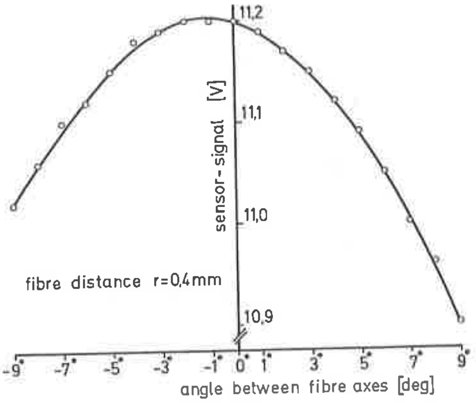


Fig. 4: Angular dependency of fibre signal according to equ. (3)

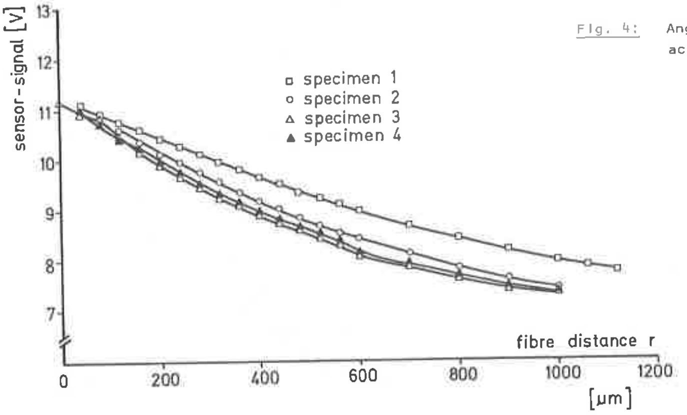


Fig. 3: Glass-fibre CTOD-meter calibration curves in CT-25 specimens

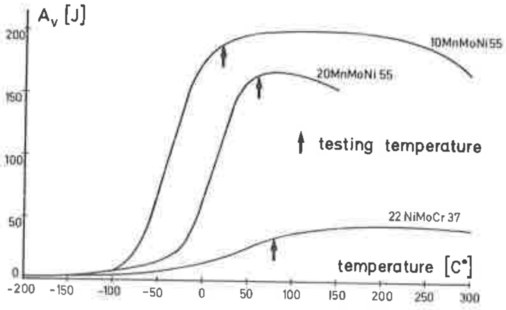


Fig. 5: Charpy V-notch impact test results

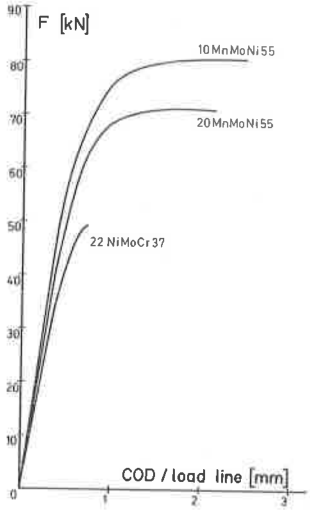


Fig. 6: Load-COD diagrams for CT 25-specimens tested

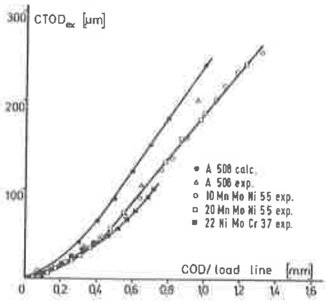


Fig. 7: Comparison of fibre-CTOD and load-line COD

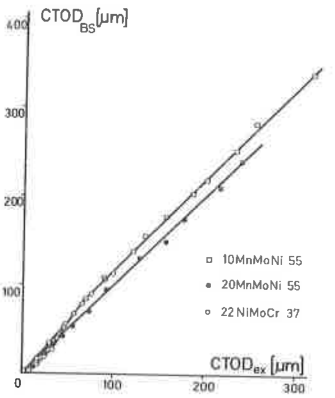


Fig. 8: Comparison of $CTOD_{BS}$, calculated according to BS 5762, and $CTOD_{ex}$, extrapolated from COD and glass fibre signal

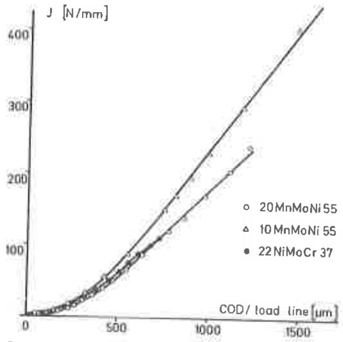


Fig. 9: J-integral vs. load line displacement COD for the materials tested

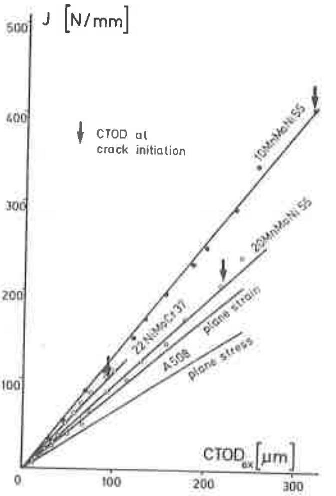


Fig. 10: J-integral vs. $CTOD_{ex}$ for the materials tested